

Extracting Shape Properties via Populations of Medial Primitives

George. D. Stetten and Stephen. M. Pizer

Medical Image Display and Analysis Group, UNC, Chapel Hill.
NSF/ERC for Emerging Cardiovascular Technologies, Duke University.

Technical Report TR98-008, University of North Carolina, Department of Computer Science

March, 1998

contact:

George Stetten, M.D., M.S.
Assistant Research Professor
Department of Biomedical Engineering
Room 136 Engineering Building
Duke University
Durham, NC 27706

phone: 919-660-5363
fax: 919-684-4488
email: stetten@acpub.duke.edu

Keywords: core, medial axis, meadialness, shape, RT3D ultrasound, 3D ultrasound.

Extracting Shape Properties via Populations of Medial Primitives

George D. Stetten and Stephen M. Pizer
Medical Image Display and Analysis Group, UNC, Chapel Hill.
NSF/ERC for Emerging Cardiovascular Technologies, Duke University.

Abstract

Various properties of 3D shape are concentrated at medial locations and can be measured efficiently and robustly using populations of medial primitives that we call core atoms. These primitives are based on a graded measurement of *medialness* with scaled apertures. Analysis of them yields a medial cloud called a *core*. The local scale, orientation, and dimensionality of a core constitute fundamental properties of an object's shape. A core with local dimensionality of zero, one, or two corresponds respectively to a local shape of *sphere*, *cylinder*, or *slab*, with non-integer dimensionality possible between these extremes.

A core atom consists of a pair of boundary points that face each other, and a *center point* midway between the boundary points. Core atom populations are grouped by their center points into bins on a 3D rectilinear grid. Each population provides a cloud-like sampling, or *coronal density*, from which the underlying regional object shape can be analyzed. This method of analysis is demonstrated here using computer generated test objects and Real Time 3D (RT3D) ultrasound scans of *in vivo* and *in vitro* targets.

Medial Primitive Populations as a Generalization of Skeletons

The lineage of the core atom may be traced to the medial axis (otherwise known as symmetric axis or skeleton) introduced on binary images by Blum and developed by Nagel, Nackman, and others [1-3]. Pizer has extended the medial axis to gray-scale images producing a graded measure called *medialness*, which links the aperture of the boundary measurement to the radius of the medial axis to produce what has been labeled

a *core* [4, 5]. Methods involving medialness and cores have proven particularly robust against noise and variation in target shape [6]. Determining locations with high medialness and relating them to a core has been accomplished by analyzing the geometry of loci resulting from ridge extraction [7]. Models including medialness have also provided the framework for a class of active shape models known as *Deformable Shape Loci* [8].

The objective of the work reported here is to build on these ideas to produce a method for analyzing the shape of the heart in Real Time 3D ultrasound, a new imaging modality that uses a matrix array of transducers elements to scan the moving heart in 3D at more than 20 frames/second [9]. The approach to analyzing this data aims to extract the scale, orientation and dimensionality (shape type) of sections of cardiac anatomy by statistical analysis of populations of medial primitives. In particular, the primitives are identified by first searching for individual boundary points throughout the image in an initial sweep, and then by matching pairs of boundary points to form what are called *core atoms*. Core atoms tend to cluster along a medial ridge and allow for statistical analysis of the core and its underlying figure. Core atoms have already been developed for analysis of 2D shape [10] and are generalized here to 3D. The analysis is also extended to spatially sampled populations of core atoms.

Methods

What is a Core Atom?

A *core atom* is defined as two boundary points \mathbf{b}_1 and \mathbf{b}_2 that satisfy particular requirements (described in detail below) that guarantee the boundaries face each other. A core atom can be represented by a single

vector $\vec{c}_{1,2}$ from the first boundary point to the second. The core atom is said to be "located" at a *center point* midway between the boundary points (see Fig. 1). The *medialness* at the center point is high because the *boundariness* at both boundary points is high and because the boundary points face each other. Core atoms carry orientation, width and position, providing the ability for populations of core atoms to be analyzed in these terms.

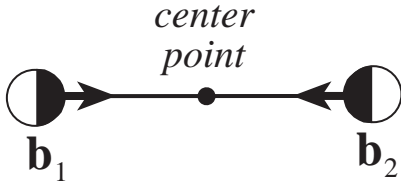


Fig. 1. A core atom consists of two boundary points that face each other across an acceptable distance, and a center point at which the core atom is said to be located.

Unlike medial models where *object angle* (half the angle between the lines from the center point to each respective boundary point) is permitted to vary, the object angle of a core atom is fixed at 90° . Core atoms thus follow in the tradition of Brady [11]. As in Brady, the underlying figure is not required to have parallel boundaries, since the boundariness detectors are assumed to show a graded response to boundary orientation.

In the experiments presented below, boundariness is based on a Difference of Gaussian (DOG) measurement of intensity gradient, accomplished by repeated application of binomial kernels. Other forms of boundariness, such as those based on texture analysis, would also be appropriate for core atoms, provided an orientation is established for the boundary.

For efficiency, boundariness vectors are sampled on a rectilinear grid, and their magnitude compared to a threshold to select a population of boundary points \mathbf{b}_i at locations \mathbf{x}_i with orientations $\hat{\mathbf{n}}_i$. The strength inherent to the statistics of populations is meant to counteract the weaknesses of thresholding. Core atoms are created from this population by finding pairs of candidate

boundary points that satisfy the following three criteria:

- (1) The magnitude of the core atom vector $\vec{c}_{1,2}$, i.e., the distance from one boundary point to the other, must be between c_{\min} and c_{\max} .

$$\vec{c}_{1,2} = \mathbf{x}_2 - \mathbf{x}_1 \quad c_{\min} \leq \|\vec{c}_{1,2}\| < c_{\max}$$

The core atom vector can be oriented either way since the order of the boundary points is arbitrary.

- (2) The boundary points must have sufficient *face-to-faceness* F defined as

$$F(\mathbf{b}_1, \mathbf{b}_2) = f_1 \cdot f_2$$

where

$$f_1 = \hat{\mathbf{c}}_{1,2} \cdot \hat{\mathbf{n}}_1 \quad f_2 = \hat{\mathbf{c}}_{2,1} \cdot \hat{\mathbf{n}}_2$$

(The " $\hat{\cdot}$ " denotes normalization, $\hat{\mathbf{v}} \equiv \vec{\mathbf{v}}/\|\vec{\mathbf{v}}\|$.) Since f_1 and f_2 are normalized to lie between +1 and -1, their product F must also lie between +1 and -1. Values for F near +1 occur when the boundaries face towards (or away from) each other across the distance between them. A threshold for acceptable face-to-faceness is set within some error ϵ_f

$$F(\mathbf{b}_1, \mathbf{b}_2) > 1 - \epsilon_f$$

- (3) Assuming $F(\mathbf{b}_1, \mathbf{b}_2) > 0$, it follows that f_1 and f_2 are both positive, or both negative. The sign of f_1 (or f_2) is called the *polarity*. The appropriate polarity is either + or - depending on whether the expected target is lighter or darker than the background.

Although at first glance the search for pairs of boundary points appears to be $O(n^2)$, hashing individual boundary points beforehand by location yields a large reduction in computation time. The search area for the *second* boundary point(s) is limited to a solid sector surrounding the

orientation \vec{n}_1 of the *first* boundary point, and to a range between c_{\min} and c_{\max} . The width of the sector depends on ε_f (see Fig. 2.)

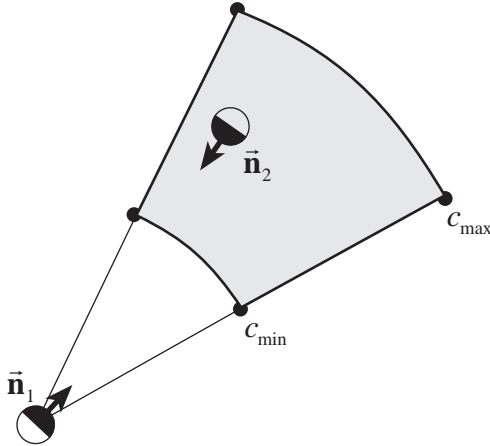


Fig. 2. The search area for the second boundary point (gray) is constrained by \vec{n}_1 , c_{\min} , and c_{\max} . The actual search area is 3D.

Three Basic Configurations: Sphere, Cylinder, and Slab

Observe that collections of core atoms can group in three basic ways corresponding to the fundamental geometric shapes shown Fig. 3. The objects are shown in dark gray with their corresponding cores shown in light gray. Beneath each object is the population of core atoms that would be expected to form with such objects, the core atoms being depicted as simple line segments.

The sphere generates a "Koosh ball" like cloud of core atoms with spherical symmetry, with the core atom centers clustered at the center of the sphere. The cylinder generates a "spokes-of-a-wheel" arrangement with radial symmetry along the axis of the cylinder, and the core atom centers clustered along the axis of the cylinder. The slab results in a "bed-of-nails" configuration across the slab, with core atom centers clustered along a plane in the middle of the slab. It is satisfying to find that the cores of these objects assume the most basic 3D shapes of all: the point, the line, and the plane.

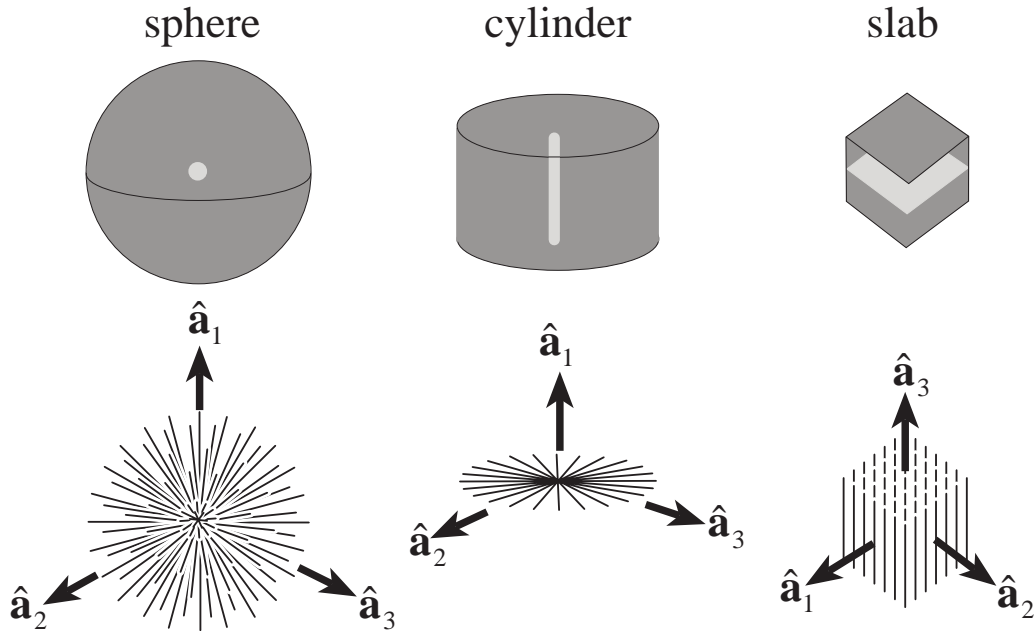


Fig. 3 - Three fundamental shapes (dark gray), corresponding cores (light gray), corresponding core atom populations (line segments) and eigenvectors \hat{a}_1 , \hat{a}_2 and \hat{a}_3 .

As shown in Fig. 3, a system of shape-specific coordinate axes, namely $\hat{\mathbf{a}}_1$, $\hat{\mathbf{a}}_2$, and $\hat{\mathbf{a}}_3$, can be assigned in each case, although the axes are not all unique given the symmetries involved. For example, in the slab, $\hat{\mathbf{a}}_1$ and $\hat{\mathbf{a}}_2$ can rotate freely about $\hat{\mathbf{a}}_3$. Such a set of coordinate axes can be found for any population of core atoms using eigenanalysis, as will be shown below. Furthermore, the extent to which any empirically determined core atom population resembles one of the three basic configurations can also be determined.

Given a population of m core atoms $\vec{\mathbf{c}}_i$, $i=1,2,3,\dots,m$, the analysis of a core atom population begins by separating each core atom vector $\vec{\mathbf{c}}_i$ into its magnitude c_i and its orientation $\hat{\mathbf{c}}_i$. We ignore, for the moment, the location of the core atom. The analysis of magnitude c_i over a population of core atoms is straightforward, yielding a mean and standard deviation for the measurement of width in the underlying figure. The orientation $\hat{\mathbf{c}}_i$ of core atoms in a population lend themselves to eigenanalysis, yielding measures of dimensionality and overall orientation for the population. We develop the eigenanalysis here in n dimensions, although for the remainder of the paper n will be 3.

Given the population of m vectors in n dimensions, it is possible to find an n -dimensional vector $\hat{\mathbf{a}}_1$ that is most orthogonal to that population as a whole by minimizing the sum of squares of the dot product between $\hat{\mathbf{a}}$ and each individual $\hat{\mathbf{c}}_i$.

$$\hat{\mathbf{a}}_1 = \arg \min_{\hat{\mathbf{a}}} \frac{1}{m} \sum_{i=1}^m (\hat{\mathbf{a}} \cdot \hat{\mathbf{c}}_i)^2$$

The normalized sum then can be rewritten

$$\hat{\mathbf{a}}^T \mathbf{C} \hat{\mathbf{a}}$$

where

$$\mathbf{C} = \frac{1}{m} \sum_{i=1}^m \hat{\mathbf{c}}_i \hat{\mathbf{c}}_i^T$$

The \mathbf{C} matrix is positive definite, symmetric, and has a unit trace. Therefore,

its eigenvalues are positive and sum to 1, and its eigenvectors are orthogonal. If the eigenvalues of \mathbf{C} are sorted $\lambda_1 \leq \lambda_2 \leq \dots \leq \lambda_n$, the corresponding eigenvectors $\hat{\mathbf{a}}_1 \dots \hat{\mathbf{a}}_n$ are the axes of a coordinate system in which $\hat{\mathbf{a}}_1$ is the most orthogonal to the population $\hat{\mathbf{c}}_i$ as a whole. For example, it would be the axis of the cylinder in Fig. 3. Furthermore, the eigenanalysis guarantees that $\hat{\mathbf{a}}_2$ is the most orthogonal to the population $\hat{\mathbf{c}}_i$ among those directions that are already orthogonal to $\hat{\mathbf{a}}_1$. This process can be repeated until $\hat{\mathbf{a}}_n$ is left as the least orthogonal to the population $\hat{\mathbf{c}}_i$, representing a form of *average* orientation for $\hat{\mathbf{c}}_i$. The axes $\hat{\mathbf{a}}_1 \dots \hat{\mathbf{a}}_n$ are thus ordered from *codimensional* (orthogonal to the vector set) to *dimensional* (collinear with the vector set). In 3D, the codimensional space is that of the core itself. That is, the space most orthogonal to the core atoms is the point, line, or plane of the core itself as shown in Fig. 3.

The Lambda Triangle

Returning now to 3D, the previous analysis yields three eigenvalues which describe the dimensionality of the core.

$$\lambda_i \geq 0 \quad \lambda_1 + \lambda_2 + \lambda_3 = 1$$

An eigenvalue of zero means that the corresponding eigenvector is perfectly orthogonal to every core atom $\hat{\mathbf{c}}_i$. Such is the case for $\hat{\mathbf{a}}_1$ in the cylinder, and for both $\hat{\mathbf{a}}_1$ and $\hat{\mathbf{a}}_2$ in the slab. In the sphere none of the eigenvectors are completely orthogonal to the core atom population. Given the symmetries of the three basic shapes, the following eigenvalues result.

sphere	cylinder	slab
$\lambda_1 = 1/3$	$\lambda_1 = 0$	$\lambda_1 = 0$
$\lambda_2 = 1/3$	$\lambda_2 = 1/2$	$\lambda_2 = 0$
$\lambda_3 = 1/3$	$\lambda_3 = 1/2$	$\lambda_3 = 1$

Since λ_3 is dependent on the other two, the system may be viewed as having only two independent variables, λ_1 and λ_2 . Because of constraints already mentioned, possible values for λ_1 and λ_2 are limited by

$$\lambda_1 \leq \lambda_2 \quad \text{and} \quad \lambda_2 \leq \frac{1-\lambda_1}{2}$$

which define a triangular domain we call the *lambda triangle*. (See Fig. 4)

The vertices of the lambda triangle correspond to the three basic shapes in Fig. 3, with all possible eigenvalues falling within the triangle. A rather crude simplification of dimensionality is possible by dividing the triangle into three compartments to provide an integer description of dimensionality. Arbitrary thresholds of $\lambda_1 = 0.2$ and $\lambda_2 = 0.33\bar{3}$ will be used to divide the triangle into such areas of integer dimensionality to clarify our experimental results. However, it should be remembered that the underlying dimensionality is not an integer or even a single scalar, but rather two independent scalars, λ_1 and λ_2 whose values are constrained by the lambda triangle.

Spatial Sampling of Core Atom Populations

We now return to the question of core atom location, which we have so far ignored. It is necessary somehow to incorporate location into the analysis of core atoms to allow for shapes whose core parameters vary along the core. Sampling a small volume provides a core atom population whose eigenanalysis yields local parameters of the core. The number of core atoms within a sample volume can be thought of as the *density* of the core at that location.

How do we choose an appropriate sample volume? Using adjacent cubical sample volumes on a rectilinear grid is straightforward and independent of the data. What size should each sample volume be? As we shall see, the local distribution of core atoms may have a significant cross section and may not be uniform within it. To preserve resolution, the sample volume may need to be smaller than the cross section

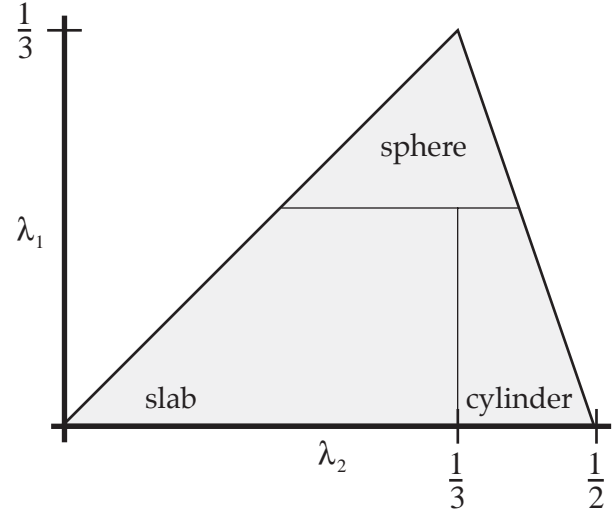


Fig. 4. The lambda triangle defines the domain of possible eigenvalues.

of the detected core. Therefore it behooves us to understand the relationship between a given sample of core atoms and the location of that sample within the cross section.

When a core is sampled off-center, it will demonstrate a distortion in its dimensionality. For example, the zero-dimensional core at the center of a sphere will appear to be one-dimensional (cylindrical) when sampled off center, as shown in Fig. 5. The vector from the theoretical core (center of the sphere) to the center of the core atom density in the sample volume is called the *displacement vector* \vec{p} (See Fig. 5C). The core atom population within a sample volume may not contain the entire thickness of the core, but rather a sub-sampling of the core called a *coronal density*. One can expect in general to be sampling coronal densities.

We can predict certain relationships to exist between the distribution of core atoms over the entire core and that of a sample volume displaced from the center of the core. The population of core atoms will be flattened in a plane perpendicular to \vec{p} , and thus develop orthogonality to that direction. This can be seen in Fig. 5, where the spherical distribution of core atoms in 5B has been flattened into a cylindrical distribution in 5C. The same effect in the case of the cylinder

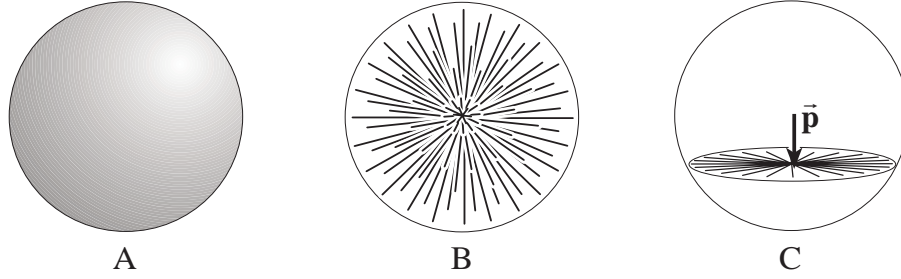


Fig. 5. **A.** spherical object. **B.** complete set of core atoms
C. cylindrical coronal density displaced by \vec{p}

can be seen in Fig. 6, where, displaced off the central axis of the cylinder by \vec{p} , the population of core atoms becomes slab-like and orthogonal to \vec{p} . One expects the displacement vector to be one of the core's eigenvectors at the closest point on the theoretical core, because (1) the displacement vector will be orthogonal to the core at that point, and (2) the normal to the core is always one of its eigenvectors. In 3D, the core can have at most 2 dimensions and thus will always have such a normal. At the theoretical core, the eigenvalue in the direction of the displacement should be 1/3 for a sphere, 1/2 for a cylinder, and 1 for a slab. As one moves out along the displacement vector, the corresponding eigenvalue should drop towards zero as the density develops orthogonality to \vec{p} , except in the case of the slab, in which the core atom population can be expected to fall off rather abruptly without significant flattening.

In the case of the cylinder, the core itself has a definite axis, which is not true for either the sphere or the slab. As can be seen in Fig. 6B and 6C, the core axis is preserved in the

coronal density, i.e., the slab-like density of core atoms displaced by \vec{p} preserves the orthogonality to the axis of the cylinder that is observed in the population as a whole. We will test these expectations in the following section.

Experimental Validation

This section reports on experiments to validate the methods developed above by applying them to three parametric test objects with simple geometries: a sphere, a torus, and a spherical shell. The torus is basically a cylinder of varied and known orientation, and the spherical shell is likewise a slab of varied and known orientation. The methods were also applied to RT3D ultrasound scans of a fluid-filled balloon in a water tank and the left ventricle (LV) of an *in vivo* human heart. The balloon and the LV are both considered roughly ellipsoidal. The goal of these experiments is to test the general approach, rather than measure its comparative accuracy and robustness against other approaches. Moreover, we only test our ability to

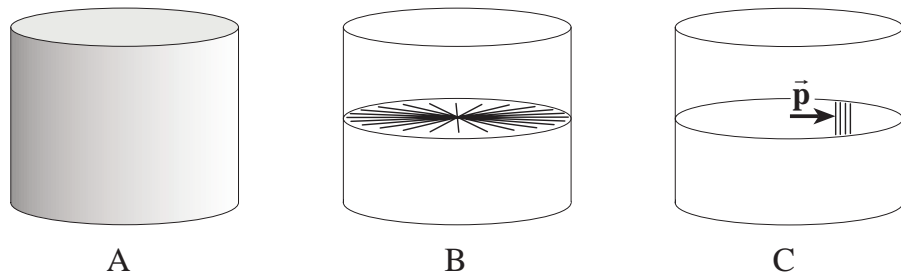


Fig. 6. **A.** cylindrical object. **B.** complete set of core atoms
C. slab-like coronal density displaced by \vec{p}

determine whether a local section of an overall geometry is roughly spherical, cylindrical, or slab-like. We expect later work will put these together into a global analysis.

Coronal Densities Displaced from a Theoretical Core

For each test object (sphere, torus, and hollow sphere, balloon and LV) the location, scale, orientation, and dimensionality of a theoretical core was calculated, and \vec{p} was derived for any test location (it being simply the displacement from the nearest point on the theoretical core to the test location). The balloon and LV were assigned a cylindrical axis by manual placement of end-points within the data, and the selection of boundary candidates was limited to an expected range of distances from that axis. For the LV the apex of the ventricle and the mitral valve served as the end-points of the axis.

Densities of core atoms collected in a rectilinear grid of sample volumes were analyzed in terms of their agreement with the theoretically correct value of diameter, orientation, or dimensionality. Some of the results are plotted in terms of the displacement magnitude $\|\vec{p}\|$ from the theoretical core. Since it cannot be expected that eigenanalysis of a coronal density will yield an eigenvector whose orientation exactly matches \vec{p} as was predicted in the previous section, a measure of angular error ε_θ is used to select that eigenvector which best matches the displacement vector, this eigenvector being called the *displacement eigenvector* \hat{a}_p .

$$\varepsilon_\theta = \arccos|\hat{a}_i \bullet \hat{p}|.$$

$$\hat{a}_p = \arg \min_{\hat{a}_i} \varepsilon_\theta \quad i = 1, 2, 3$$

For cylindrical cores, an *axial eigenvector* \hat{a}_a was also chosen as being the closest eigenvector to the theoretical axis of the core.

Experimental Results

A measurement of diameter was made for each test object by averaging the diameter

from all densities whose integer dimensionality matched that of its theoretical core. Thus only spherical densities were considered for the sphere, etc. Actual diameters were known for the parametric test objects, and roughly estimated by eye for the balloon and LV, having no single definable diameter. The results are shown in the following table.

MEASUREMENT OF DIAMETER				
object	dim.	actual	measured	
			mean	s.d.
sphere	0	70	69.20	0.08
torus	1	25	23.90	0.07
sph. shell	2	25	22.30	1.50
balloon (mm)	1	40*	35.10	4.60
LV (mm)	1	40*	42.50	8.90

* approximate, by eye

Eigenanalysis of the coronal densities collected over a rectilinear grid of sample volumes yielded the following results. Fig. 7 shows all densities containing greater than 1% of the entire core atom population plotted on a lambda triangle. The sphere shows two clusters, one near the top (sphere) vertex of the triangle and another near the right (cylinder) vertex, consistent with the dimensional effects of the corona predicted in Fig. 5. The torus, which is locally a cylinder, shows clustering near the right (cylinder) vertex, with some spreading towards the left (slab) consistent with the dimensional effects of the corona predicted in Fig. 6. The spherical shell, which is locally a slab, shows tight clustering at the left (slab) vertex consistent with the observation that core atoms in a slab are collinear with \vec{p} and will therefore not develop significant orthogonality.

The balloon and LV in Fig 7 each show a more dispersed cluster of densities than the parametric test objects. Their dimensionality seems to be roughly between sphere and cylinder, with the LV being somewhat more cylindrical than the balloon, which is consistent with their observed shapes.

Fig. 8-12 show the density (number of core atoms) in each sample volume as a function of displacement magnitude from

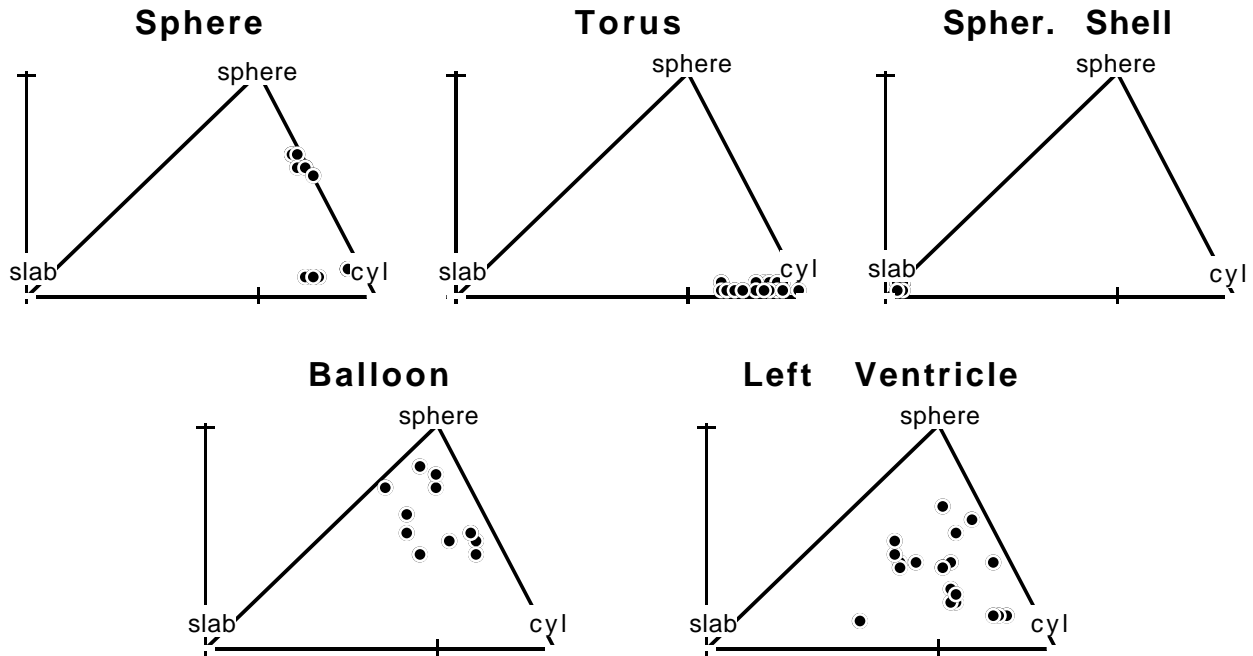


Fig. 7 Coronal densities containing more than 1% of the total number of core atoms (see Fig. 4).

the theoretical core. In all cases the density is concentrated near the theoretical core (c.f. diameters under each graph). Integer dimensionality ($\circ = 0$, $\times = 1$, $+ = 2$) behaves as expected in the sphere, torus and spherical shell, clearly showing the predicted distortion of dimensionality with displacement in the first two cases. Again, the slab shows no such distortion. For the balloon and LV the results are less clear cut, but still consistent with general expectations.

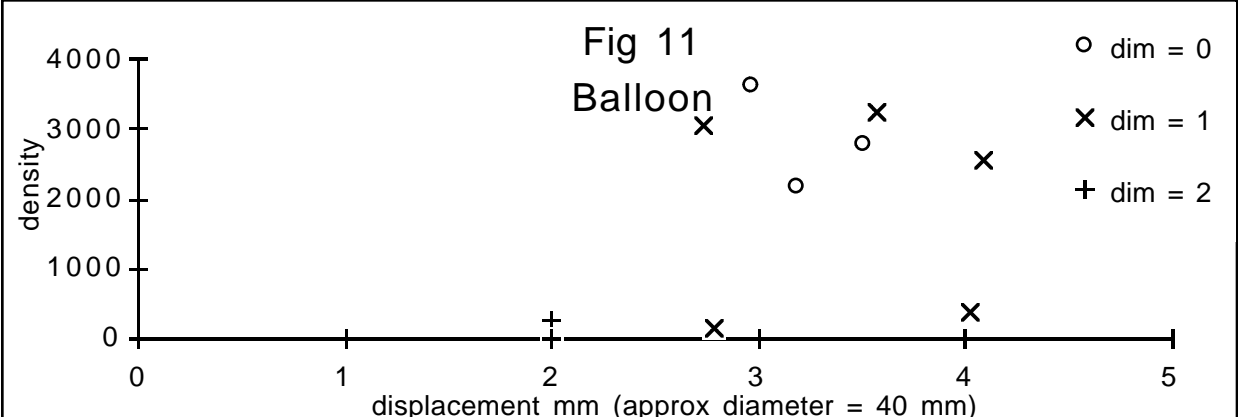
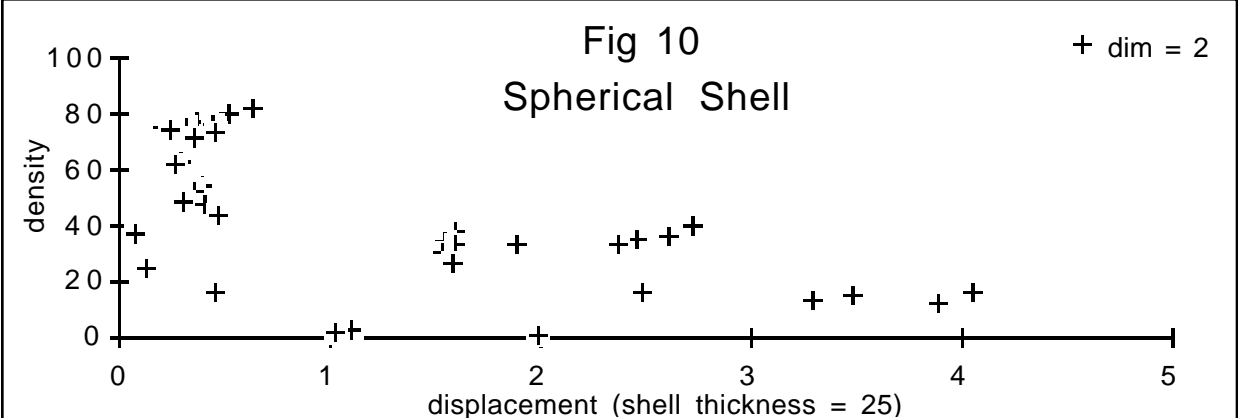
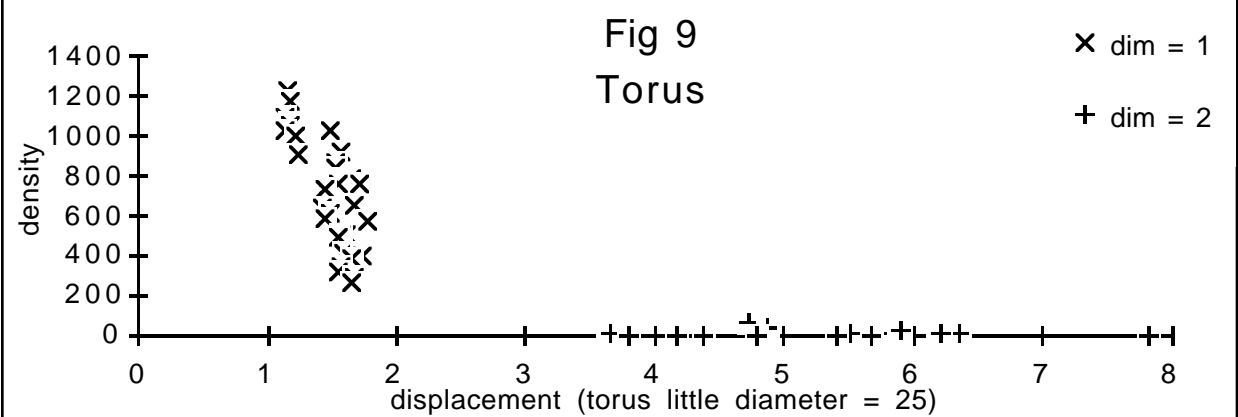
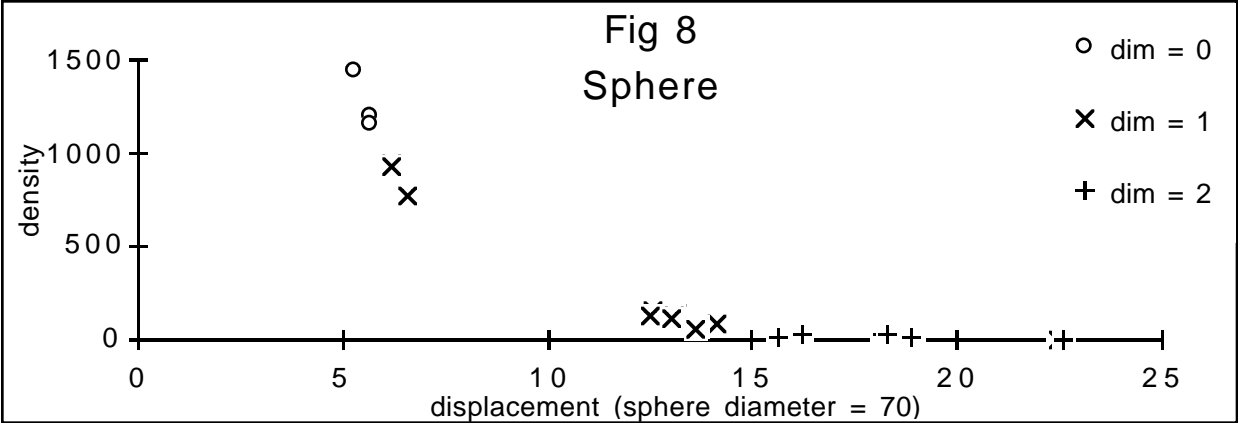
Fig. 13-15 show the eigenvalue associated with the displacement eigenvector $\hat{\mathbf{a}}_p$ as a function of displacement. In all cases (except a few aberrant points for the torus) the eigenvalue behaves as expected, dropping to zero with increasing displacement for the sphere and torus, with the y-intercept roughly consistent with $1/3$ for the sphere, $1/2$ for a cylinder, and 1 for a slab. As expected, the eigenvalue for the slab does not drop off with displacement.

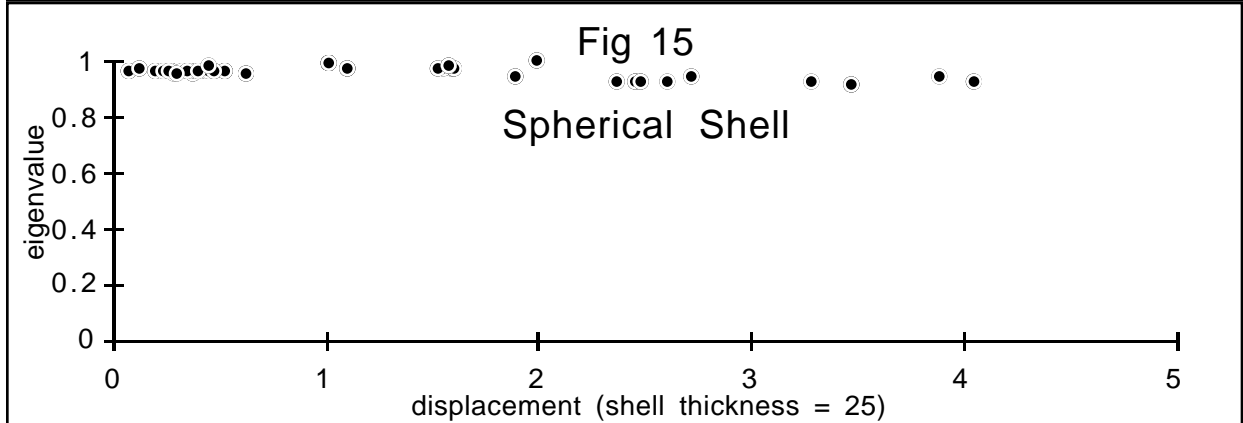
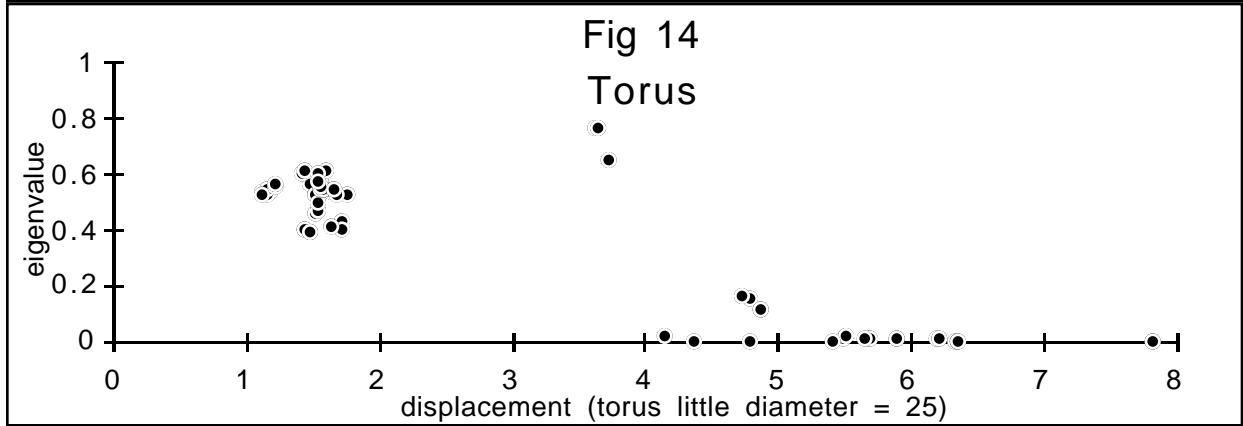
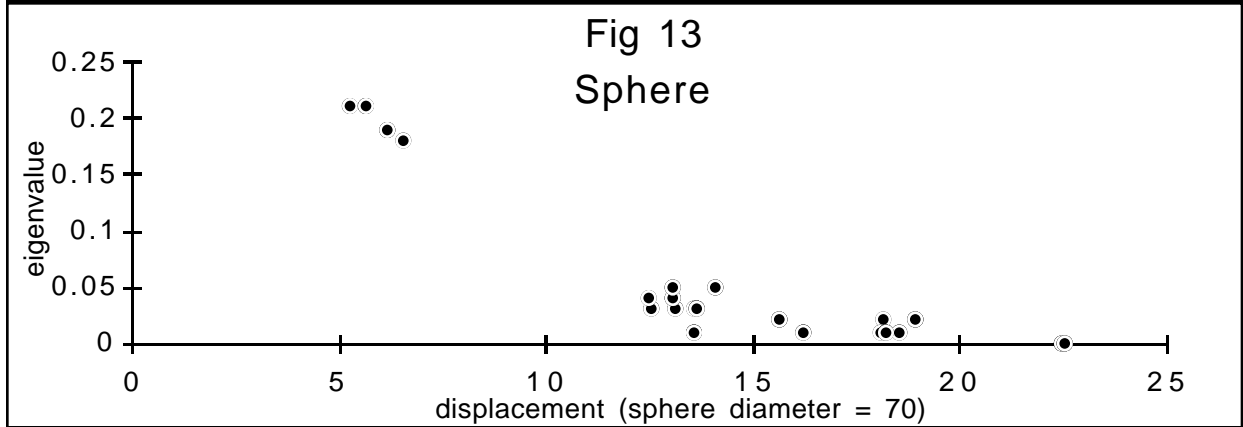
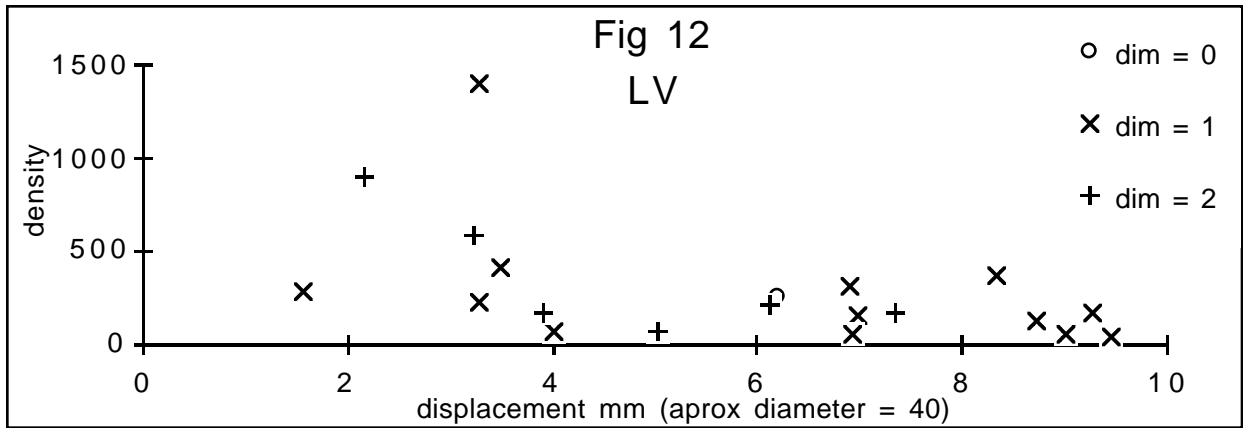
Mean angular error $\bar{\epsilon}_\theta$ over the sampled densities (weighted by density) is reported in Table 2. The displacement eigenvectors $\hat{\mathbf{a}}_p$ of sample densities are oriented with high

accuracy for the sphere and the spherical shell, while the torus shows high accuracy in the alignment of the axial eigenvector $\hat{\mathbf{a}}_a$. The symmetry of the cylinder (torus) allows the $\hat{\mathbf{a}}_p$ to rotate freely at the core. This may explain the increased $\bar{\epsilon}_\theta$ for the $\hat{\mathbf{a}}_p$ of the torus as well as the aberrant points in Fig. 14. Results for the balloon and LV are somewhat indeterminate.

MEAN ANGULAR ERROR $\bar{\epsilon}_\theta$		
	$\hat{\mathbf{a}}_p$	$\hat{\mathbf{a}}_a$
sphere	6.1	-
torus	23.1	5.1
spherical shell	2.7	-
balloon	28	24.2
LV	21.5	29.7

Table 2. Mean angular error $\bar{\epsilon}_\theta$ (in degrees) for displacement eigenvector $\hat{\mathbf{a}}_p$, and axial eigenvector $\hat{\mathbf{a}}_a$ (cylinders only).





Conclusions

This paper establishes relationships between coronal densities and the underlying theoretical core using parametrically defined objects with known cores of integer dimensionality. It further demonstrates the general feasibility of applying such techniques to real ultrasound data.

One potential use of this approach is to generate a measure of LV volume, heart wall thickness, or other important anatomical parameters. Another is to provide a robust and efficient means of landmark identification. Understanding the relationship between a theoretical core and its coronal densities may permit the design of algorithms to optimize the fit of a theoretical core, which could then be matched against a model for automated identification of anatomical landmarks.

Acknowledgments

Supported through a Whitaker Biomedical Engineering grant, NSF grant CDR8622201 NIH grants 1K08HL03220, P01CA47982, and HL46242, with help from 3D Ultrasound, Inc., and Silicon Graphics.

References

- [1] H. Blum and R. N. Nagel, "Shape description using weighted symmetric axis features," *Pattern Recognition*, vol. 10, no. pp. 167-180, 1978.
- [2] L. R. Nackman, "Curvature relations in 3D symmetric axes," *CVGIP*, vol. 20, no. pp. 43-57, 1982.
- [3] L. R. Nackman and S. M. Pizer, "Three-Dimensional shape description using the symmetric axis transform I: Theory," *IEEE PAMI*, vol. 2, no. 2, pp. 187-202, 1985.

- [4] C. A. Burbeck and S. M. Pizer, "Object representation by cores: Identifying and representing primitive spatial regions," *Vision Research*, vol. 35, no. 13, pp. 1917-1930, 1995.
- [5] S. M. Pizer, D. H. Eberly, B. S. Morse and D. S. Fritsch, "Zoom invariant vision of figural shape: the mathematics of cores.," *Technical Report TR96-004, University of North Carolina, 1996. To appear in Computer Vision and Image Understanding*, vol. no. pp. 1996.
- [6] B. S. Morse, S. M. Pizer, D. T. Puff and C. Gu, "Zoom-Invariant vision of figural shape: Effect on cores of image disturbances.," *draft, Department of Computer Science, UNC Chapel Hill.*, vol. no. pp. 1996.
- [7] J. D. Furst and S. M. Pizer, "Marching Cores: A method for extracting cores from 3D medical images.," *Proceedings of the Workshop on Mathematical Methods in Biomedical Image Analysis, San Francisco, CA, June 1996.*
- [8] D. Fritsch, S. Pizer, L. Yu, V. Johnson and E. Chaney, "Segmentation of Medical Image Objects Using Deformable Shape Loci," *Information Processing in Medical Imaging, Poultney, Vermont, 1997.*
- [9] G. Stetten, T. Ota, C. Ohazama, C. Fleishman, J. Castelucci, J. Oxaal, J. Kisslo and O. T. v. Ramm, "Real-Time 3D Ultrasound: A New Look at the Heart," *J. Cardiovasc. Diagnosis and Proc.*, vol. no. pp. (in press, May, 1998).
- [10] G. Stetten, R. Landesman and S. Pizer, "Core-Atoms and the spectra of scale, (Technical Report TR97-006, UNC Dept. Computer Science," *SPIE Medical Imaging Conference, 1997.*
- [11] M. Brady, Criteria for representations of shape., New York, Academic Press, 1983.